# Demonstration of a Multi-Layer, Lithographically Manufactured Plasma Spectrometer

**E. E. Scime,[1]M. Dugas,[2]T. J. Gilbert,[1]R. John,[1]A. M. Keesee,[3]and G. Wagner[2]**

[1]Department of Physics and Astronomy, West Virginia University, Morgantown WV 26506
[2]Advanced Research Corporation, White Bear Lake, MN
[3]Department of Physics and Astronomy, University of New Hampshire, NH

## Key Points:

- Microscale plasma energy analyzer demonstrated in laboratory tests
- Lithographic fabrication process enables low voltage analysis of charged particles up to tens of keV/charge
- Multi-layer instrument required development of a novel fabrication process

Corresponding author: E. Scime, escime@wvu.edu

**Abstract**

Development of new plasma instruments is needed to enable constellation- and small satellite-based missions. Key steps in the development pathway of ultra-compact plasma instruments employing lithographically patterned wafers are the implementation of layer-to-layer electrical interconnects and demonstration of massively parallel measurements, i.e., simultaneous measurements through multiple identical plasma analyzer structures. Here we present energy resolved measurements of electron beams using a 5-layer stack of wafer-based, energy-per-charge, electrostatic analyzers. Each layer has eight distinct analyzer groups that are comprised of multiple micron scale energy-per-charge analyzers. The process of fabricating the electrical interconnects between the layers is described and the measured energy resolution and the angular resolution compared to theoretical predictions. The measurements demonstrate successful operation of 400 micron scale analyzers operating in parallel.

## Plain Language Summary

Spacecraft are expensive and difficult to build. CubeSats, a class of small, inexpensive spacecraft are being used for scientific missions. However, standard instruments to measure the local plasma environment cannot fit on such small spacecraft. Here we describe a new type of space plasma instrument that is manufactured with processes similar to how computer chips are made. These plasma instruments are made by stacking layers of micro-scale plasma analyzers to create a larger instrument with a significant geometric factor. Each layer includes nearly one hundred small energy-per-charge plasma analyzers working in parallel. Initial measurements from a 5 layer instrument along with the processes used to build the instrument are described in this work.

## 1 Introduction

Whether through opportunistic conjunctions or design, exploration of near-Earth space has increasingly focused on understanding the energy flow and coupling between different spatial regions through simultaneous measurements of essential plasma parameters, e.g., magnetic field, electric field, density, and temperature, over the relevant spatial length scales. The International Solar Terrestrial Physics (ISTP) program's Wind, Polar, and Geotail missions(Desch et al., 1997; Pulkkinen et al., 1997) and the THEMIS mission(Angelopoulos, 2008) provided new insights and global perspectives on the flow of energy from the solar wind through the magnetosphere. Though highly successful, those missions were limited by rare conjunctions and sampling of only one place in each region of the magnetosphere and upstream solar wind. Recent missions, e.g., Magnetospheric Multiscale Mission (MMS)(Burch et al., 2016) and SWARM (Macmillan & Olsen, 2013) have employed multiple spacecraft to resolve local gradients in plasma parameters and to investigate kinetic scale phenomena. Such spatially resolved measurements are critical for understanding the electrodynamics of different parts of the magnetosphere.

Upcoming missions, e.g., Helioswarm(Klein et al., 2023), will take advantage of advances in the capabilities of CubeSat-scale instruments to minimize costs while launching a constellation of 9 spacecraft. The 9 spacecraft CINEMA mission concept also recently advanced to the next round of NASA SMEX mission studies.(NASA, 2023) Looking beyond these scientific missions, it is possible to imagine deploying plasma instruments on hundreds to thousands of spacecraft if either the spacecraft are mass-produced at low cost or if the instruments require so little resources that they could be included on commercial spacecraft with little to no impact on the operation of those spacecraft. With a truly massive (in number) constellation of instruments, it would be possible to obtain simultaneous, high spatial resolution, vector field and plasma measurements over a significant fraction of the magnetosphere. Such measurements could also be used as inputs into real-time models of the near-Earth space environment.

However, the last generation of conventional plasma spectrometers, e.g., those flown on MMS(Pollock et al., 2016), are too massive (roughly 6 kg), consume too much electrical power (several Watts), and require too much assembly and testing time to be flown on future multi-spacecraft microsatellite missions (total spacecraft mass less than 10 kg and total power less than 5 W (Frost, 2014)). The plasma instruments being developed for Helioswarm require significantly reduced resources, but they are still manufactured in the "classic" sense - through machining of metal parts and manual assembly. Advanced wafer scale fabrication techniques naturally lend themselves to relatively high manufacturing volumes and therefore change the paradigm for dealing with flaws or defects in individual instruments. In other words, if it is possible to mass produce one thousand low-cost plasma instruments, faulty units are simply thrown away and replaced with a functional instrument before integration with the spacecraft.

There are essentially three elements in any plasma instrument: a collimating structure that defines the field-of-view and, ideally, provides partial or complete shielding of the instrument from sunlight; an energy per charge or energy per mass resolving analyzer (this element could also be a simple time-of-flight detector that only measures particle velocity); and a detector sensitive to charged particles in the desired energy range. In previous studies we demonstrated the successful integration of a collimating structure with an electrostatic analyzer at the wafer-scale level(Scime et al., 2016a, 2016b; Keesee et al., 2018). Here we report the successful integration of multiple wafer layers and demonstration of a functional, massively parallel, energy-per-charge electrostatic analyzer.

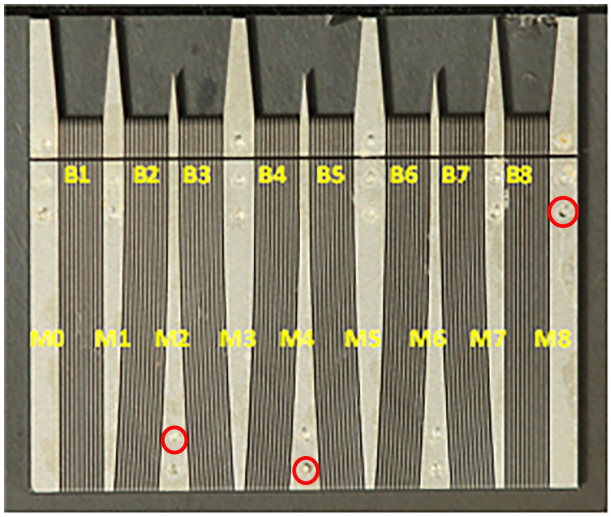


**Figure 1.** Photograph of a single Collimator and Energy Analyzer wafer or "layer." Across the top of image, the collimator section of the wafer is electrically isolated from the curved plate analyzer section. There are 8 energy analyzer bands, numbered from left to right, which consist of 10 channels (80 $\mu$m wide) created by 9 fins (60 $\mu$m wide). The outer two energy analyzer bands in this test wafer have straight channels for alignment purposes. The inner six bands have curved fins with a radii of 15 mm. The "mesas" in between the bands are the structures through which electrical interconnections are made. Barely visible in this image are the "through-silicon via" holes in the mesas that go through the glass substrate to complete the wafer-to-wafer connections. Three of the "through-silicon via" features are circled in red.

## 2 Instrumentation

### 2.1 Single Layer Energy Analyzer and Collimator

Shown in Fig. 1 is a single layer combined Collimator and Energy Analyzer (CEA) wafer or "layer." Every CEA wafer consists of eight electrostatic analyzer (EA) bands, each with its own collimator section (top) that is mechanically and electrically isolated from the EA section (bottom). Each EA band consists of 10 curved channels (80 $\mu$m wide) created by 9 fins (60 $\mu$m wide and 360 $\mu$m tall) with radii of 150 mm. Charged particles enter at the top of the wafer, are collimated by the fins of the collimator section, travel through the curved energy analyzer channels for energy selection, and then exit the bottom of the wafer to a detector. In this prototype wafer, the outer EA bands are straight to facilitate alignment during testing. For the curved bands, charged particles of energy, $E$, and charge, $q$, will pass through a channel of spacing, $\Delta r$, and radius of curvature, $R$, for a voltage difference, $V$, across the channel such that

$$E = qV/(2ln(1 + \Delta r/R)). \tag{1}$$

For closely spaced plates, Eq. 1 reduces to $E = (qR\Delta V/(2\Delta r))$ to first order. Thus, for 5 keV electrons, $\Delta r = 80\mu$m, and $R = 150$ mm, the required voltage difference across each gap is $V = 5.33$ Volts. To obtain that voltage across each gap, a total voltage difference of 53.3 V is needed across the entire band of 10 channels. The collimator consists of identically spaced fins and outer tapered structures that limit the angular acceptance of the flux entering each band to a nominal range of $\pm 5^\circ$. An important feature of each wafer is that since the collimator fins are completely aligned with the EA fins, the effective transparency of the collimator is 100%. Typically, the transparency of the collimator is an additional loss term when calculating the total throughput (geometric factor) of a plasma instrument. The collimator angular acceptance helps to define the energy resolution of each band by limiting the range of possible trajectories through the plates for charged particle energies that do not satisfy Eq. 1. Note also that the energy analysis is accomplished with only modest voltages. Therefore, for the analyzer portion of the instrument, no high voltage power supplies are required - which makes construction of a variable energy analyzer bias supply (to sweep across multiple particle energies) considerably easier. Because the potential difference applied between two plates is at most a few volts, it is impossible to create an electrical discharge in between the plates even though the electric field between two plates is large enough to deflect charged particles of energies up to tens of keV/e (the voltage difference between any two plates is comparable to or smaller than the ionization potential of atmospheric gasses and therefore an ionization cascade is difficult to initiate).

The CEA chips were fabricated using a proprietary Deep Reactive Ion Etching (DRIE) recipe developed by our team. The fins are etched in 360 $\mu$m thick, heavily P/Boron doped silicon on a 200 $\mu$m glass substrate. The glass substrate serves as an etch stop and also maintains electrical isolation. The bands in Fig. 1 are numbered 1-8 from the left and the "mesas" between the bands are numbered from 0 to 8, again from the left. The highly conductive silicon used for the fins and mesas has an electrical conductivity comparable to aluminum. A CEA built for a flight instrument would have all eight EA bands with curved fins and with varying bias voltages applied to each band to obtain a eight-point energy spectrum during each measurement interval. Since each energy band is continuously sampled, the duty factor for the energy analyzer at each energy is 100%. Note the small circular features in the mesas in Fig. 1. Those features are the "through-silicon via" (TSV) holes drilled through the entire wafer and then filled with a conductive material to create the wafer-to-wafer electric connections. The overall dimensions of the CEA in Fig. 1 are 1.8 cm wide, 1.5 cm high, and 0.056 cm thick.

An ideal curved plate electrostatic analyzer would have curved fins that subtend an angle of $127°(\pi/\sqrt{2})$ to obtain first-order focusing of charged particles at the image (detector) plane. The CEA shown here subtends a much smaller angle (just enough to require photons to make a single bounce to pass through the instrument). Therefore, the energy resolution of this instrument is worse than the nominal energy resolution of $\Delta E/E \sim \Delta r/R$ for an ideal curved plate analyzer, where $\Delta E$ is half the full width of the transmission function. The energy resolution could be improved by increasing the angle subtended by the curved fins at the expense of a more complicated geometry at the exit plane of the wafer.

### 2.2 Wafer Stacking

The full instrument is designed to employ 25 of these individual CEA wafers in a single vertically integrated energy analyzer. Using double-sided lithography, a thin gold electrode pattern with the same width and spacing of the fins and mesas is deposited on the underside of each CEA wafer. In the collimator region, the entire underside region is a single ground plane. The TSV holes connect the mesas to the electrode pattern on the underside of the wafer. There are multiple TSV connections in each mesa to ensure a robust electrical connection. A boron hydride wire is deposited across the entire underside electrode structure and serves as a voltage divider for each of the fins. The fin and mesa structures on each wafer are coated with a 100 $\mu$m thick capping layer to couple the silicon structures to the electrode pattern on the underside of the wafer above. With the addition of a final electrical breakout layer on the top of the stack, the full 25 set of wafers is placed into a alignment mechanism and bonded together. Shown in Fig. 2 is bonded set of 25 incompletely processed (so they are not fully functional) wafers. The clear glass substrates facilitate viewing of the entire bonded structure.

**Figure 2.** Photograph of a bonded stack of 25 incompletely processed test wafers, each on a glass substrate. The dimensions of the full 25 stack are 1.8 cm wide, 1.5 cm deep, and 1.65 cm high.

To minimize current draw, the boron hydride resistor has a nominal mesa-to-mesa resistance of 1.4 MΩ. With the voltage divider in place and assuming all eight energy

bands consistent of curved fins, six unique potentials applied to mesas 0-8 in a pattern of 100 V, 50 V, 75 V, 0 V, 12.5 V, 17.5 V, 20 V, 0 V, and 100 V create nominal energy passbands of 5 keV/e, 2.5 keV/e, 7.5 keV/e, 1.25 keV/e, 0.5 keV/e, 0.25 keV/e, 2 keV/e, and 10 keV/e, respectively. Including the thickness of the capping layer, the dimensions of the full 25 stack in Fig. 2 are 1.8 cm wide, 1.5 cm deep, and 1.65 cm high. For comparison, a typical sugar cube has sides of 1 cm. Note that the 8 energy bands in all 25 layers operate in parallel. Therefore, a detector with 8 discrete regions of sensitivity placed behind the energy analyzer (as shown in Fig. 3) would collect flux from all 25 layers simultaneously. The conceptual detector shown in Fig. 3 is a commercially available 8 pixel solid state detector. To overcome the energy threshold of the solid state detector, there would need to be a postacceleration potential of 15- 20 kV applied between the exit of the analyzer and the front of the detector (or relative to a high transmission grid placed in front of the detector). In this conceptual instrument design, the spacing between the energy bands (and the overall width of each wafer) has been slightly modified to match the spacing of the detector pixels in the commercial off-the-shelf (COTS) detector.

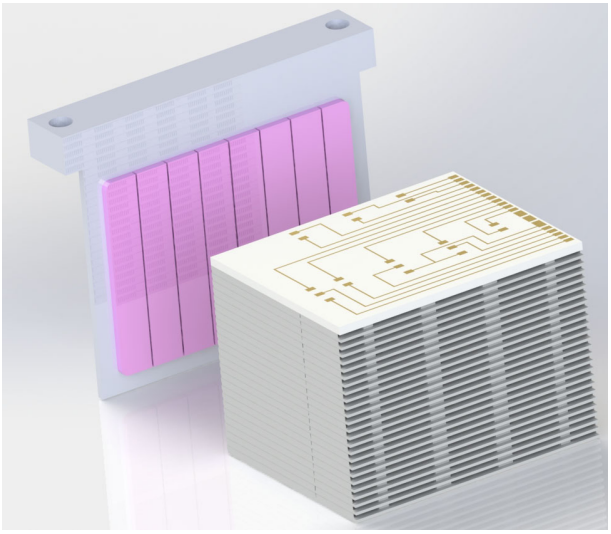

**Figure 3.** A schematic of 25 energy analyzer layers with an eight pixel solid state detector roughly 1 cm beyond the exit of the analyzer. The gap is placed between detector and analyzer so that a post acceleration potential of 10-20 kV between detector and analyzer will not arc across the gap. To match the spacing of the detector pixels, the band-to-band spacing in each of the wafers in this conceptual model has been increased slightly from that in Fig. 2.

## 3 Measurements of Electron Fluxes Through a 5-Layer Stack

As a first step in demonstrating the functionality of a multi-layer instrument, a fully functional 5-stack assembly was fabricated, bonded into a single structure, and a ribbon cable mounted to the top electrical breakout layer. Each of the wafers was a prototype wafer as shown in Fig. 1, i.e., each wafer has 6 inner curved fin analyzer bands and the outer two bands have straight fins. A full 5-stack assembly is shown in Fig. 4. A Quantar imaging microchannel plate (MCP) detector was mounted behind the 5-stack assembly to image the flux of charged particles that passed through the energy analyzer. To prevent electrons from reaching the MCP directly, additional shields and a layer of aluminium foil were placed around the 5-stack assembly. The entire assembly was then illuminated with a variable energy electron beam (1 - 5 keV). Before the measurements, the electron beam profile was measured with just the MCP to optimize the beam uni-

formity at the location of the measurement. The imaging MCP has a spatial resolution of approximately 65 $\mu$m (the size of each channel in the MCP sensor).

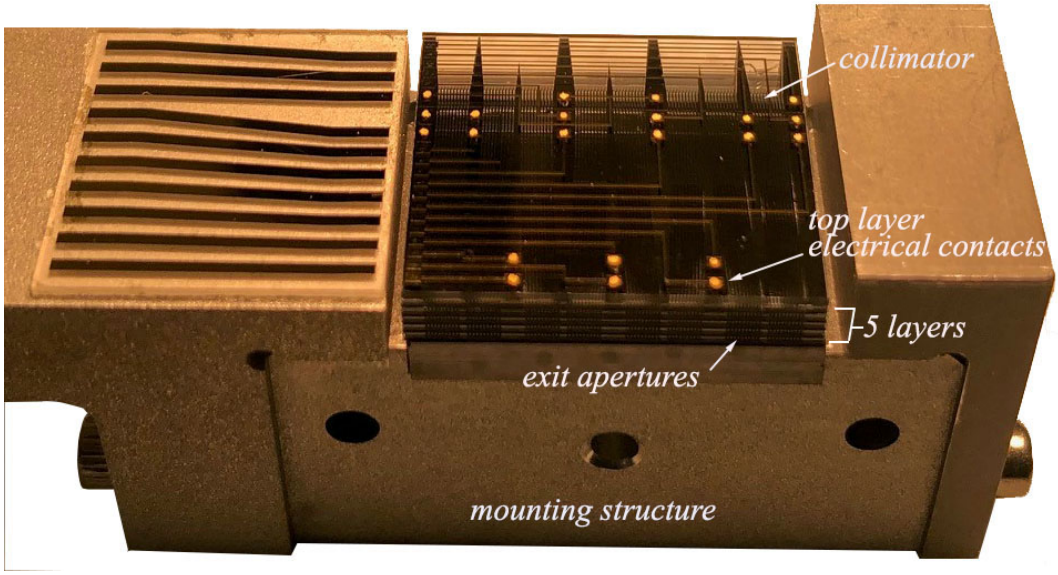


**Figure 4.** An annotated photograph of a fully functional 5-layer stack before it was wired. The 5-layer stack is mounted on a test structure to which an imaging microchannel plate (MCP) detector is later mounted.

Shown in Fig. 5 are two MCP images of the flux of 3 keV electrons passing through the 5-stack assembly for a voltage difference of 37 V applied to the inner six bands and 0 V applied across the outer two bands. There are a number of important features in these figures. First, the maximum flux through the energy analyzer was obtained at exactly the bias potential predicted by Eq. 1. Second, in Fig. 5a, there are three clearly identifiable layers through which flux is passing. In Fig. 5b, the the fourth layer appears in all four signal regions. There is a hint of a fifth layer in the two signal regions to the right of the image. Because of the coarse nature of the tilt angle stage to which the 5-stack assembly was mounted, it was difficult to reliably align the assembly so that all 4 (sometimes 5) layers were illuminated. The angular precision needed, as will be discussed later, was less than 1°. In the initial measurements, there was a thin piece of aluminium foil that was placed near the top layer of the analyzer when the image in Fig. 5a was recorded. It is possible that the foil was blocking the top two layers. The foil was removed for the image in Fig. 5b, but all five layers were still not visible. Two other issues could have prevented full illumination of all 5 layers. First, when the electrical breakout layer at the top of the stack was bonded to the stack, it is possible that some of the capping layer material seeped into the channels of the bands. Second, there is a modest divergence of the electron beam. Thus, electrons with a velocity component perpendicular to the beam axis will be blocked by the relatively narrow angular acceptance of the energy analyzer. In practice, the ambient electron populations in space are superthermal and electron flux comes from all directions around the instrument. In other words, an instrument like this in space would be illuminated from all directions and beam divergence issues would not impact performance.

Another important feature in the images is that only four regions of signal appear instead of the eight that would be expected for the eight energy bands. Notice also that the outer signal regions are significantly wider than the two inner signal regions. The

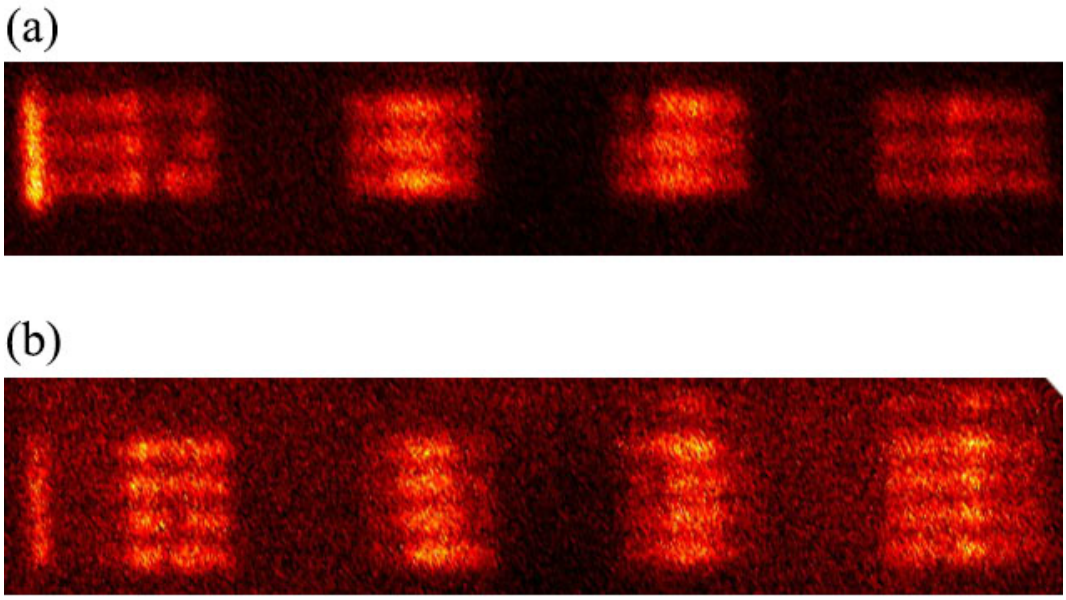


**Figure 5.** Imaging microchannel plate (MCP) measurements of 3 keV electron flux through a 5-stack energy analyzer. (a) Electron beam illuminating the lower 3 layers of the 5-stack. (b) After removal of some blocking aluminium foil and more careful alignment of the 5-stack assembly to the electron beam, 4 full layers were seen across all 8 bands and hints of the $5^{th}$ layer are evident in the two signal regions to the right of the image.

measured flux pattern results from the serendipitous placement of the MCP detector relative to the exits of the eight energy bands. Comparing the measured flux pattern to the energy band locations shown in Fig. 1, it is clear that the inner two signal regions result from the overlap of energy bands with opposite curvatures. By placing the MCP at the distance at which the flux exiting two bands fully overlap, the signal from both bands is measured at the same location on the MCP. To passively separate the flux from the two bands, the imaging MCP would have to be placed much closer to the exits of the 5-stack (before the fluxes overlap) or much further away (after the fluxes pass through each other and become distinguishable again. SIMION™simulations of the combined energy analyzer and detector assembly shown in Fig. 3, show that active separation of the fluxes from two bands of opposite curvature is possible if a 10-20 kV post-acceleration potential is placed at the exit of the energy analyzer. The fluxes from adjacent curved channels are then easily directed to distinct regions on the segmented detector. The two outer signal regions in Fig. 5 are wider because for this prototype energy analyzer, the two outermost energy bands have straight fins. Therefore, fluxes from an outer band and the curved band next to it are adjacent but do not fully overlap for the energy analyzer-to-MCP spacing used in these measurements. Thus, the signal regions from left to right in Fig. 5 are from $(B1 + B2), (B3 + B4), (B5 + B6)$, and $(B7 + B8)$.

To confirm that the energy selection properties of the 5-stack were consistent with predictions based on the geometry of the structures, the potential difference required to maximize the transmitted electron flux was measured for four different electron beam energies. All of the energy bands were set to transmit the same beam energy and only the fluxes transmitted through the inner four energy bands were measured. As shown in Fig. 6a, the bias voltage measurements for the 5-stack energy analyzer are well fit by a linear relationship. The slope of the fit yields an applied bias to energy per charge scaling relationship that is within 10% of the predicted value. As noted previously, the en-

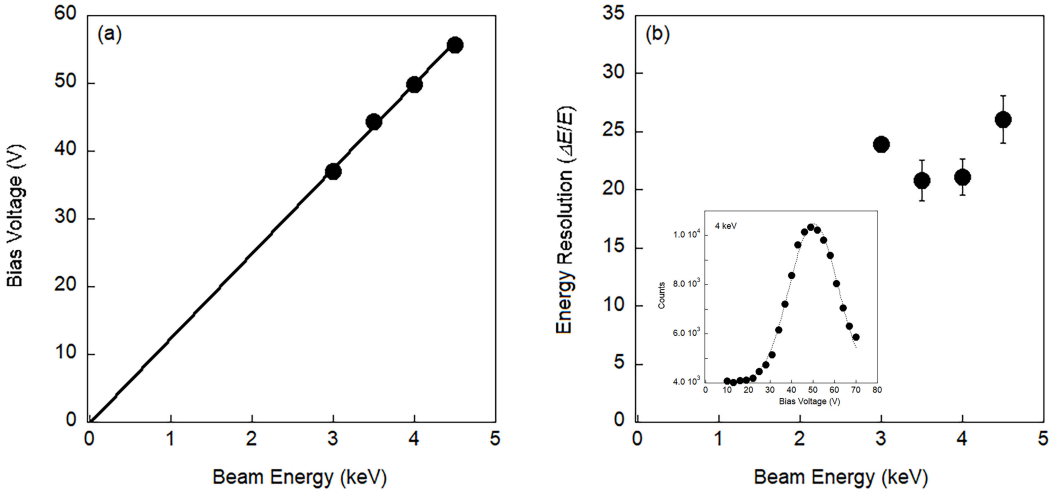


**Figure 6.** (a) Energy analyzer bias voltage required to maximize the transmitted flux as a function of electron beam energy. The solid line is the predicted scaling of the energy analyzer (Eq. 1) a function of transmitted beam energy. (b) Measured energy resolution as a function of beam energy. Each measurement is based on measurements of the transmitted electron flux for a fixed beam energy versus energy analyzer bias voltage, e.g. the 4 keV beam example shown in the insert.

ergy resolution of each energy band is worse than it would be for an ideal 127° analyzer. Based on SIMION$^{TM}$ simulations of a full energy band structure, the expected energy resolution of a single analyzer band is approximately 20%. Shown in Fig. 6b are the measured energy resolutions for four different electron beam energies transmitted through the inner four energy bands. Each measurement is based on the HWHM of a Gaussian fit to the measured flux for a fixed beam energy ($\Delta V/V$) as a function of bias voltage applied to the energy analyzer (see insert in Fig. 6b). The relatively poor energy resolution results from the limited curvature of each fin. The nominal 20% energy resolution is, however, completely consistent with the modeling predictions and previous measurements of single layer transmission (Scime et al., 2016a, 2016b).

The transmitted electron flux for a beam energy of 3 keV as a function of rotation angle around the normal to the plane of layer (azimuthal angle) and the tilt angle of the wafer relative to the axis of the electron beam (pitch) are shown in Fig. 7a and b, respectively. Again, only the transmitted fluxes for the four inner energy bands were used in the measurements. For the azimuthal angle measurements, the expected angular resolution is estimated from the fin-to-fin spacing and the overall length of each curved fin (the collimator acceptance of ±5° is much larger than the angular acceptance of each curved pathway). From $\tan\theta = \Delta r/L$, where $L = 100$ $\mu$m, the estimated azimuthal angular acceptance is ±0.5°. A Gaussian fit to the transmitted flux data of Fig. 7a yields measured azimuthal angular acceptance of ±0.79° - slightly larger than the predicted value. The angular acceptance of the instrument in the pitch direction should be much larger than in the azimuthal direction because the height of the fins is roughly four times larger than the fin-to-fin spacing. However, the measured angular acceptance in the pitch direction (Fig. 7b) is comparable to the azimuthal angular resolution ($\sim$ ±0.89°). The measurements are of modest quality since, as noted previously, the motion stage used for the pitch angle measurements had poor resolution and repeatability in the pitch direction. Hints of similar results for pitch angular acceptance were reported in previous measurements of a single CEA layer(Keesee et al., 2018). The reason for the limited pitch

angular resolution is not clear. The MCP images (Fig. 5) suggest that electrons are coming through the full vertical span of the channels when the entrance apertures are fully illuminated, at least for 4 of the layers. One possibility is that the electron beam divergence in the pitch direction is larger than assumed. However, the previous single CEA layer measurements and these 5-stack measurements employed different electron beam sources, so it is unlikely that both sources had anomalously large beam divergences in the pitch direction.

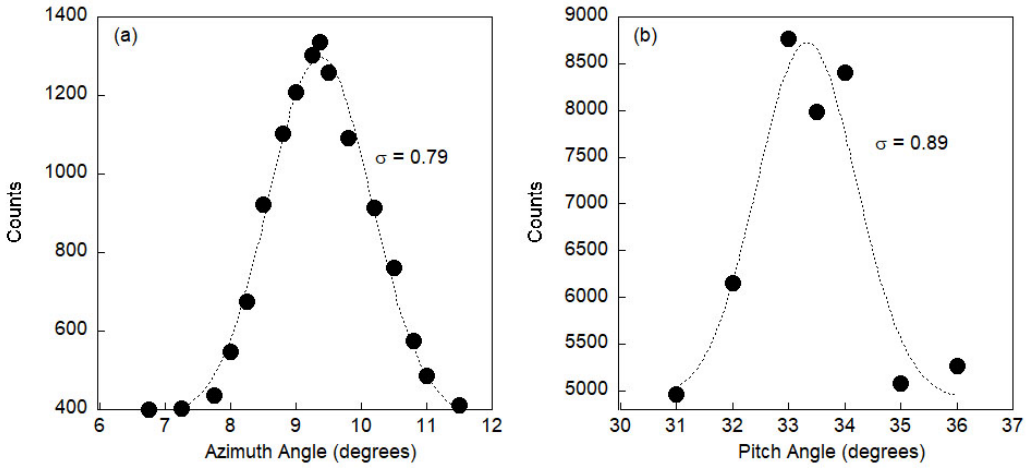


**Figure 7.** (a) Transmitted flux through the inner four energy bands as a function of azimuthal angle (rotation axis around the normal to the layers). (b) Transmitted flux through the inner four energy bands as a function of pitch angle (tilt of the layer plane relative to the nominal beam direction).

## 4 Conclusions

A multi-layer, lithographically fabricated plasma spectrometer has been fabricated and demonstrated to accurately measure the energy per charge of a 1 - 5 keV electron beam. The 5-layer instrument demonstrated is a prototype of a 25 layer instrument that will have nominal dimensions of 1.5 x 1.5 x 1.5 $cm^3$. The 5-layer prototype consisted of 400 individual $E/q$ analyzers operating in parallel to create a miniaturized instrument with an estimated per pixel (per viewing direction), per energy band, geometric factor on the order of $G = 1.6 \times 10^{-5} cm^2$ sr (eV/eV) for the full 25 layer instrument (Scime et al., 2016a). For comparison, the FPI instrument for MMS has a geometric factor of $G = 2 \times 10^{-4} cm^2$ sr (eV/eV) per imaging pixel at 20 keV (Collinson et al., 2012). In other words, were the full 25-layer instrument to be placed into the same orbit as the MMS spacecraft, the expected count rate in each imaging direction would be 10% of that of the FPI instrument.

To increase the spatial coverage or the overall geometric factor of this type of instrument, a collection of these ultra-compact plasma spectrometers could be used in parallel. Note that the geometric factor of this type of instrument scales linearly with any dimension of the instrument, whereas conventional instruments grow in volume as the surface area of the aperture increases. In other words, one hundred, e.g., a 10 by 10 array, of these ultra-compact plasma spectrometers placed on the side of a CubeSat would have a geometric factor ten times larger than a conventional plasma spectrometer but would still only be a panel approximately 15 cm x 17.5 cm in area and 1.5 cm thick. All one hundred ultra-compact spectrometers could share the same power supplies and read-

out electronics. Were all six sides of a single unit CubeSat to be covered with such panels, such a collection of plasma spectrometers could provide six measurements through a full three-dimensional particle velocity distribution with a substantial count rate.

We note that the energy per charge scaling, angular resolution, and energy resolution of the energy analyzer are in excellent agreement with the design targets. The fabrication steps developed to make the electrical interconnections between the layers were successful and these results demonstrate that multi-layer, lithgraphically fabricated plasma spectrometers are ready to be mated to solid state detectors with postacceleration to create robust instruments amenable to large-volume manufacturing.

## Open Research Section

The data that support the findings of this study are openly available in Zenodo at https://doi.org/10.5281/zenodo.8406445.

### Acknowledgments

This work supported by NASA Grant 80NSSC19K0490. We thank our colleagues at UNH Chris Bancroft and Jim Connell for helpful discussions regarding solid state detectors and Shane Cupp at WVU for assistance with the electron gun.

## References

Angelopoulos, V. (2008, DEC). The themis mission. *SPACE SCIENCE REVIEWS*, *141*(1-4), 5-34. doi: 10.1007/s11214-008-9336-1

Burch, J. L., Moore, T. E., Torbert, R. B., & Giles, B. L. (2016, MAR). Magnetospheric multiscale overview and science objectives. *SPACE SCIENCE REVIEWS*, *199*(1-4), 5-21. doi: 10.1007/s11214-015-0164-9

Collinson, G. A., Dorelli, J. C., Avanov, L. A., Lewis, G. R., Moore, T. E., Pollock, C., ... Adrian, M. L. (2012, 03). The geometric factor of electrostatic plasma analyzers: A case study from the Fast Plasma Investigation for the Magnetospheric Multiscale mission. *Review of Scientific Instruments*, *83*(3), 033303. Retrieved from `https://doi.org/10.1063/1.3687021` doi: 10.1063/1.3687021

Desch, M., Ogilvie, K., Acuna, M., Fairfield, D., & Hoffman, R. (1997, APR 15). Early multiplatform results from the international solar terrestrial physics global geospace science (istp/ggs) program. *GEOPHYSICAL RESEARCH LETTERS*, *24*(8), 913. doi: 10.1029/97GL00837

Frost, C. (2014). Small spacecraft technology state of the ar. *NASA/TP–2014–216648/REV1*.

Keesee, A. M., Dugas, M., Ellison, S., Neal, L., Scime, E. E., Thompson, D. S., ... Tucker, C. J. (2018, 08). Micro-spectrometer for fusion plasma boundary measurements. *Review of Scientific Instruments*, *89*(10), 10J116. Retrieved from `https://doi.org/10.1063/1.5035365` doi: 10.1063/1.5035365

Klein, K. G., Spence, H., Alexandrova, O., Argall, M., Arzamasskiy, L., Bookbinder, J., ... Zweibel, E. (2023, June). HelioSwarm: A Multipoint, Multiscale Mission to Characterize Turbulence. *arXiv e-prints*, arXiv:2306.06537. doi: 10.48550/arXiv.2306.06537

Macmillan, S., & Olsen, N. (2013). Observatory data and the swarm mission. *EARTH PLANETS AND SPACE*, *65*(11), 1355-1362. doi: 10.5047/eps.2013.07.011

NASA. (2023). *Cinema mission.* Retrieved from `http://website-url.com` (October 12, 2023)

Pollock, C., Moore, T., Jacques, A., Burch, J., Gliese, U., Saito, Y., ... Zeuch, M.

(2016, MAR). Fast plasma investigation for magnetospheric multiscale. *SPACE SCIENCE REVIEWS*, *199*(1-4), 331-406. doi: 10.1007/s11214-016-0245-4

Pulkkinen, T., Baker, D., Turner, N., Singer, H., Frank, L., Sigwarth, J., ... Slavin, J. (1997, APR 15). Solar wind magnetosphere coupling during an isolated substorm event: A multispacecraft istp study. *GEOPHYSICAL RESEARCH LETTERS*, *24*(8), 983-986. doi: 10.1029/97GL00816

Scime, E. E., Barrie, A., Dugas, M., Elliott, D., Ellison, S., Keesee, A. M., ... Tersteeg, J. (2016a, FEB). Key elements of a low voltage, ultracompact plasma spectrometer. *JOURNAL OF GEOPHYSICAL RESEARCH-SPACE PHYSICS*, *121*(2), 1452-1465. doi: 10.1002/2015JA022208

Scime, E. E., Keesee, A. M., Dugas, M., Ellison, S., Tersteeg, J., Wagner, G., ... Elliott, D. (2016b, 08). A micro-scale plasma spectrometer for space and plasma edge applications (invited). *Review of Scientific Instruments*, *87*(11), 11D302. Retrieved from `https://doi.org/10.1063/1.4960145` doi: 10.1063/1.4960145